Computers, Materials & Continua CMC, vol.65, no.1, pp.945-962, 2020

Research on Clothing Simulation Design Based on Three-Dimensional Image Analysis

Wenyao Zhu[1, 2], Xue Li[3] and Young-Mi Shon[4, *]

Abstract: Traditional clothing design models based on adaptive meshes cannot reflect. To solve this problem, a clothing simulation design model based on 3D image analysis technology is established. The model uses feature extraction and description of image evaluation parameters, and establishes the mapping relationship between image features and simulation results by using the optimal parameter values, thereby obtaining a three-dimensional image simulation analysis environment. On the basis of this model, by obtaining the response results of clothing collision detection and the results of local adaptive processing of clothing meshes, the cutting form and actual cutting effect of clothing are determined to construct a design model. The simulation results show that compared with traditional clothing design models, clothing simulation design based on 3D image analysis technology has a better effect, with the definition of fabric folds increasing by 40%. More striking contrast between light and dark, the resolution increasing by 30%, and clothing details getting a more real manifestation.

Keyword: 3D image, analysis clothing simulation, feature extraction, optimal solution, mapping relationship, collision detection, grid layout, cutting effect.

1 Introduction

Three-dimensional image technology is one of the most advanced computer display technologies in the world. Most ordinary computers only need to install a plug-into present three-dimensional products in a web browser [Hu and Hou (2017)]. Not only is it realistic, but also dynamically displays the combination process of products [Ribeiro, Janssen and De (2017)]. Remote browsing eliminates the expense and time for sending samples in the marketing process [Sun, Li and Lowe (2017)]. Products that are not portable can be displayed to customers on computers, which greatly enhances the competitiveness of the products [Deng, Fitts and Peters (2017)]. Three-dimensional images are popular in the use of people's visual differences and optical refraction principle in a plane to make people see a three-dimensional map directly, which can be

[1] College of Engineering, Lishui University, Lishui, 323000, China.

[2] Department of Design, Graduate School, Chosun University, Gwangju, 61452, Korea.

[3] Department of Materials Science and Engineering, Graduate School, Chosun University, Gwangju, 61452, Korea.

[4] Design Division, College Art & Design, Chosun University, Gwangju, 61452, Korea.

[*] Corresponding Author: Young-Mi Shon. Email: nbzhn06@163.com.

Received: 10 February 2020; Accepted: 25 April 2020.

convex out of the picture and also be hidden in it vividly in a strong visual impact [Keall, Ng, Juneja et al. (2017)]. It is essentially different from the plane image. The plane image reflects the two-dimensional relationship between the object and the upper and lower sides [Kim, Modrick, Pennington et al. (2017)]. This is mainly embodied in the use of light and shadow, virtual reality and contrast of light and shade. The real stereoscopic painting is the principle of simulating the world by the human eyes [Majchrowicz, Kapusta, Jackowskastrumiłło et al. (2017)]. It is made of optical refraction. It can make the eyes see the three-dimensional relations of objects up and down, left and right, before and after [Yong, Kim and Yong (2017)]. It is a three-dimensional painting in real visual sense. The emergence of three-dimensional technology is another technological revolution in the field of image color replacing black and white. It is also the future trend of the image industry [Bannas, Li and Motosugi (2017)]. The stereoscopic image industry is the gold industry in twenty-first Century, which is praised as "the cradle of time and money" by experts [Nitzken, Beache and Ismail (2017)]. A perfect three-dimensional map is composed of two or more layers, visually distinct and colorful, and has a strong visual impact by showing people real characters, with immersive feeling and high art appreciation value [Karlsson, Thunberg and With (2017)].

At present, although many researches have been conducted at home and abroad, the fast and ideal garment simulation is still a challenge [Schwerter, Lietzmann and Schad (2017)]. The basic steps of adaptive mesh clothing simulation include multiple processes such as fabric modeling, motion control, collision detection, and response processing [Chen, Ni and Peng (2017)]. This method completes the summarization and generalization of the virtual clothing simulation technology through the local adaptive subdivision and merging method of triangular meshes [Wang, Wei and Chen (2017)]. However, with the advancement of science and technology, this method cannot truly reflect the true details of the clothing [Yepes, Gesualdi and Yepes (2017)]. In order to solve this problem, clothing simulation design model based on three-dimensional image analysis technology is established [Gaich and Pötsch (2017)], and the establishment of the model operating environment is completed through single mapping relationship establishment method [Lie, Trivedi and Mukhopadhyay (2017)]. Through the analysis and comparison of experimental data, it can be seen that the new garment simulation design model does have a high practical value [Matsubara and Hashimoto (2017)].

The specific contributions of this paper include:

(1) The establishment of clothing simulation design model based on 3D image analysis technology and the mapping relationship between image features and simulation results by using the optimal parameter value, have thereby established a 3D image simulation analysis environment.

(2) By obtaining the response results of the clothing collision detection and the results of the local adaptive processing of the clothing mesh, the cutting form and actual cutting effect of the clothing were determined, thereby completing the construction of the new design model.

(3) Good results were obtained through simulation: Compared with the traditional clothing design model, the clarity of fabric folds was improved after applying the clothing simulation design model based on 3D image analysis technology. The contrast between light and dark was more obvious, with the details of the clothing being truly reflected.

2 Three-dimensional image simulation analysis environment

The 3D image simulation analysis environment is the basis of the operation of the apparel design model. The specific construction process can be performed as follows.

2.1 Image Feature Extraction and Description

Three-dimensional image feature extraction is often performed in several steps: (1) Feature formation. Based on the identified objects, a set of original features are generated, which can be either the direct measurement of the sensor or the value obtained by some calculation of the measurement value of the sensor [Grosser, Wybranski and Kupitz (2017)]. (2) Feature selection. There may be many original features acquired through the feature formation process. If all the original features are sent to the classifier as a classification feature, not only is the classification process is complicated, but there are also a large number of discriminant classification calculation, and the probability of classification error is not necessarily small, so it is necessary to reduce the feature dimension [Goreczny, Dryzek and Moszura (2017)]. Feature selection is the selection of subsets for classification based on a criterion (singling out some of the most effective features) from a collection of many different features metrics as a classification feature of dimension reduction. (3) Feature extraction. Feature extraction is another method to reduce the dimension of features. It is to make many feature measures through some kind of mathematical transformation to generate fewer feature measures. Their purpose is to reduce the dimension of the feature space in order to achieve the effective classification while preserving the image information as much as possible.

For the image gray image, after a series of feature extraction processing, the possible target in the image has been separated from the background, and the result is generally two value images. As the remaining target features are few, generally, target recognition is achieved through the shape of the target. There are two ways to express the shape of a target: skeleton and edge. Contour extraction is more robust and faster than skeleton extraction, which contains most of the information of the target shape as the first choice for identifying features. The method of describing the boundary contour of the target is: the length of the contour is defined as the number of pixels of the contour curve; the contour diameter is defined as the maximum distance between two points on the contour, also called the long axis of the contour; the minor axis of the contour is defined as a straight line that is perpendicular to the major axis; the eccentricity of the profile is defined as the ratio of the major axis to the minor axis; there are statistical invariant moments, fourier descriptors, and curvature-based descriptors. In the actual three-dimensional image automatic target recognition process, the representation of the contour feature is required to have translation, rotation, and scale invariance, and even to satisfy the affine invariance [Fang, Ding, Zhang et al. (2019)]. The latter three description methods have the most extensive application in practice due to their good expression and recognition performance.

$$c = \sqrt{\frac{a+2b}{\chi}} \tag{1}$$

In which, c is image feature parameters, a stands for garment feature description

factor, b represents related clothing material parameters, and χ represents stationary extraction of original parameters [Wu, Liu and Lou (2019)]. If Δu represents the subjective quality of the image, it can extract the amplitude of parameter variation [Fang, Zhang, Victor et al. (2019)].

$$\Delta u = \sqrt{\frac{\tau}{d}\left|1+\frac{fg}{o}\cdot\frac{(h-1)\varepsilon^4}{\iota^3}\right|} \tag{2}$$

In which, d is the subjective evaluation coefficient of three-dimensional image, τ is the number of quality extraction, o is the sensory measurement value of the image, f is the disassembly parameter of three-dimensional image. g is the original value of the state of the three-dimensional image points in the target image resolution layer, h is the upper limit of the rated range of change, ε is the fixed extraction coefficient, and ι is the original value of the fixed point.

2.2 Optimal solution of image evaluation parameters

The traditional image quality evaluation methods mainly include objective evaluation and subjective evaluation. The objective evaluation is generally to count the pixel values of the image and use the statistics to describe the image quality. The typical statistics include the gray average value, the gray variance, the mean square error and so on. However, the results obtained by statistics are often inconsistent with subjective visual effects. This is because whatever the statistic is, it is an overall reflection of the image and does not reflect the local difference, such as a statistical result that may be equal in the difference between a large gray level and a larger image point with a smaller gray level. Obviously, the same treatment of all the image points in the image cannot reflect the human visual characteristics. The subjective evaluation method is to allow the observer to judge the quality of the test image according to the evaluation scale or experience of its own, and give the quality score, namely, the weighted average of the scores given by all the observers. The result is the subjective quality evaluation of the image. There are two scales for subjective evaluation, that is, absolute scale and relative scale, as shown in Tab. 1. Although this measurement method reflects the visual quality of the image, it cannot be described by mathematical model. From the perspective of engineering application, it is too time-consuming and laborious. In practice, the subjective quality evaluation method of images is severely restricted, and even is not suitable for some applications, such as real-time image transmission,and it is not even suitable for real-time image transmission.

Table 1: Subjective quality measurement score table

Level	Absolute measurement scale	Relative measurement scale
1	Very poor	The worst in the group.
2	Poor	Worse than the average level in the group.
3	Commonly	Average level in the group.
4	Preferably	Better than the average level in the group.
5	Very good	The best in a group.

The optimal solution results of image evaluation parameters mainly include two aspects: first, the reconstruction of three-dimensional images is evaluated to complete the description of reconstruction distortion. The quality of image evaluation directly affects the quality of the final three-dimensional image, with the core to find appropriate evaluation function. Second, the searching method of the optimal solution to the parameter requires the fastest solution to obtain the optimal solution, whose accuracy of the parameter solution is based on the image evaluation. The meaning of image quality mainly includes two aspects: the fidelity and the intelligibility of the image. Research on image quality evaluation has become one of the basic technologies of image information engineering. It is expected that a quantitative measure of image fidelity and intelligibility can be found as a basis for evaluating images and simulating image designs. However, people still do not fully understand human visual characteristics. In particular, it is difficult to find a quantitative description of the psychological characteristics of human eyes. Therefore, image quality evaluation needs further study. The optimal solution of the specific image evaluation parameters is shown in formula (3).

$$J(i) = \sum_{0}^{r\to\infty} (i + \lambda\Delta u)di \tag{3}$$

In which, J is the optimal solution of the image evaluation parameter, i is the image feature variable to be integrated, r is the upper limit of the image quality level, and λ is the image gray scale coefficient.

2.3 Three-dimensional simulation mapping relationship description

The description process of the three-dimensional simulation mapping relationship includes seven steps: target initial calibration, rotation scanning, parameter initialization, two-dimensional slice image correction, three-dimensional data reconstruction, three-dimensional image evaluation, and adjustment of parameter values. Among them, the goal of the initial calibration step is to make the ultrasound beam emission center of the image monitoring probe and the axis of rotation of the stepping motor approximately in a straight line, so that the introduced parameter change is limited to a small range and the volume of the center data less cone is reduced to eliminate the search range for subsequent parameters. The specific method is: firstly bind a pencil on the shaft of the motor. As the motor rotates, a circle can be drawn out with a pencil. Find the center of the circle by finding the center of the circle on the geometry, which is the projection of the mechanical axis of rotation on the circle plane. This method can theoretically make the center of ultrasonic beam emission and the axis of rotation of the stepping motor in a straight line, called this coarse calibration because:

(1) The axis of rotation of the mechanical axis is not necessarily perpendicular to the plane of the circle.

(2) The needle itself is not necessarily perpendicular to the plane of the circle.

(3) The length and diameter of the needle will affect the image in the three-dimensional image, which will in turn affect the judgment of whether it is on a straight line.

Based on the initial calibration of the three-dimensional image target, the

two-dimensional sequence image data is acquired. At this time, the error of the centerline of the ultrasonic probe and the axis of the rotary shaft of the stepping motor is not coincident, with the possible range being limited to a small area. As the acquisition of two-dimensional sequence image data is performed at the same time as scanning, and analog image on the display screen of the ultrasonic machine is digitally collected by the image capture card, which are sequentially stored in the memory of the personal computer. In this process, attention should be paid to the matching of the speed of rotation scan, the speed of probe data acquisition and the speed of acquisition card, so as to satisfy the sampling theorem and achieve a more satisfactory resolution.

The parameter initialization process is mainly aimed at the optimal solution of the image evaluation parameters, and the solution process can finally be attributed to a search process. First of all, these parameter values are all set to zero and assumed to be a special ideal state without errors, from which the initial state begins to search for the actual position of the imaging plane of the probe. Two-dimensional slice image correction is to complete the conversion of the pixel coordinated of the oblique two-dimensional slice image and the spatial regular coordinated to realize the symmetry of the data. From the ideal error-free reconstruction method, it is demonstrated that the three-dimensional image is based on the principle of the two-dimensional cross-sectional image with the motor's axis of rotation around the center of the motor. considering the ultrasound probes centerline and rotation axis heartline of the stepper motor is coplanar but not collinear, the reconstruction is based on the body element layer by layer. This tilting and translation break this symmetry, making it more complicated to search for the nearest four pixels around each voxel and the positional relationship, and complicating the entire three-dimensional reconstruction process. Therefore, it is an indispensable step to rectify the left and right tilt and asymmetry of the original image relative to the mechanical axis of rotation, and to construct a two-dimensional image containing the acquired data with the axis of rotation as the axis of symmetry. The actual position of the three-dimensional image of the skirt when it is not collinear is shown in Fig. 1.

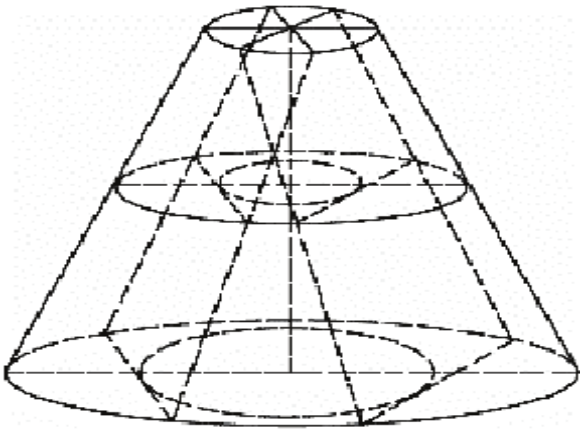

Figure 1: Actual position diagram when the three-dimensional image of the skirt is not collinear

As can be seen from Fig. 1, the actual positional relationship between the mechanical rotation axis of the three-dimensional image of the skirt and the center of the two-dimensional slice image is not collinear. The three-dimensional data reconstruction step completes the calculation of the gray value of each voxel in the three-dimensional image, and the specific operation process follows Eq. (1). The evaluation of the three-dimensional image is performed. As if the preset image standard has been reached, the obtained three-dimensional image is used as the reconstructed image, and the algorithm is terminated; otherwise, the seventh step is entered. When the parameter values are chosen improperly, they cannot describe the true spatial position of the imaging plane of the probe, thus resulting in the distortion of the reconstructed three-dimensional image. The result of image evaluation should reflect the magnitude of this distortion. When the degree of distortion is small enough to meet the required reconstruction accuracy, the parameters used can correctly represent the spatial position of the 2D image. The result of image evaluation is the basis of parameter adjustment. Different parameter adjustment rules have different parameter optimization methods.

3 Clothing design model building based on 3D environment

On the basis of the three-dimensional image simulation analysis environment, a new type of clothing simulation designed model is built through the operation process of fabric collision detection and response.

3.1 Fabric collision detection and response

The core of fabric collision detection algorithm for the new garment simulation design model is to determine whether some parts of two objects collide with the current position by effectively traversing the clothing bounding box tree and the human model bounding box tree. This is a double recursive traversal process consisting of a recursive function Traverse Tree, where *C* is the current node in the costume bounding box tree and *H* is the current node of the human bounding box tree. The original inputs of the algorithm are the root node *C* in the clothing bounding box tree and the root nodes *H*, S and S, *H* of the human form bounding box tree, which are subsets of the basic geometric elements corresponding to the nodes *C* and *T*, respectively. The collision effect is up to the rated requirement. The recursive function is described as follows, and the specific operation flow is shown in Fig. 2.

$$W = \frac{Q}{1+\frac{(rl)^2}{15\eta^3}X} \cdot J(i) \tag{4}$$

In which, W is the cloth collision detection result, Q is the total cloth mass, r is the fabric response parameter, l is the model simulation coefficient, η is the probability of collision event, and X is the original collision variable. Eq. (5) is recursively processed, and its specific calculation formula is as follows:

$$X(v) = \int_{-\infty}^{\infty} W\sigma(v)e^{-\varpi}dv \tag{5}$$

In which, X represents the recursive processing result of cloth collision detection, σ represents the quantitative response to the primary response, e represents the cloth shape variable, ϖ represents the number of deformations of the clothing fabric, and v represents the attribute parameter of the clothing cloth. Jointing Eq. (6) and density function, cloth collision response results can be expressed as:

$$Z = \lim_{m \to \infty} \frac{1}{T} |X(v)\theta|^2 \tag{6}$$

In which, Z is the fabric collision response result, m is the minimum collision number, T represents the reciprocal of the collision time, and θ represents the possible twist angle of the fabric.

Figure 2: Operation flow chart of Cloth collision detection algorithm

Whenever two leaf nodes collided are detected the position on the collision point is re-adjusted according to the collision response algorithm, thereby avoiding inaccurate visual effects such as penetration. At the same time, since the expansion bounding box is used in the detection, the critical neighboring relationship is also subjected to collision reaction processing, so that multiple collisions can also obtain stable and accurate results. In the process of clothing simulation, in addition to the collision between costumes and the person model, a large number of collisions will occur on its own due to the dynamic deformation of the clothing, so further self-collision detection must be performed.

If there is a collision between the particle and the triangular patch, the position and velocity of the colliding particle is corrected according to the motion law of the

completely inelastic collision, that is, the collision response. For the position collision between the clothing particles and the human body surface, the human body surface exerts a certain force on the clothing particles to avoid the occurrence of the penetration phenomenon. The size and direction of this force is determined by the movement state of the body surface and the current movement state of the clothing particle. In addition to collision response mechanism, it is necessary to ensure that no conflict occurs between the surface of the clothing and the surface of the human body, and it is more important to change the current state of the conflicting clothing particles according to the movement state of the human body in order to obtain true simulation result. In addition, the collision response algorithm also sets a collision buffer area with a width of E on the surface of the human model to predict possible collision detection, which not only avoids the huge time cost of penetrating the lag correction and the possible instability of the simulation system, but also guarantees the accuracy of collision detection. As an empirical parameter, E can be a constant and also be dynamically adjusted according to the motion speed of the clothing particle and the human body model.

3.2 Local adaptive processing of clothing mesh

Due to the complexity of natural fabrics, cloth simulation is a costly process, and the amount of calculation directly depends on the mesh resolution. In the simulation, the mesh resolution determines the degree of refinement of the available cloth mesh, that is, the number of mass points, to a large extent, will affect the time complexity of cloth simulation. In order to produce realistic cloth simulation effects, it is often necessary to simulate local details of the cloth, such as wrinkles. It is necessary to use a fine grid, which, however, will make the computational time unacceptably high. If a coarse grid is used, the simulation is faster and more stable, but the reality will be greatly reduced. It can be seen that the unified resolution cannot meet the needs of realistic fabric simulation. The core idea of an adaptive mesh is to use different resolutions for the folded area and the smooth area of the fabric, respectively, to reduce the computational cost by avoiding the extra mosaic in the smooth area. The common adaptive refinement method is based on the spring-mass model. In this method, the angle between the two springs connecting the particles is used as a condition for refinement. When the included angle exceeds the custom threshold, the grid cells near the particle are divided into four, as shown in Fig. 3. However, since the midpoint average method is used for refinement, the newly generated particles do not inherit the properties of the original particles very well, resulting in the simulation results being not as satisfactory as possible and being inefficient.

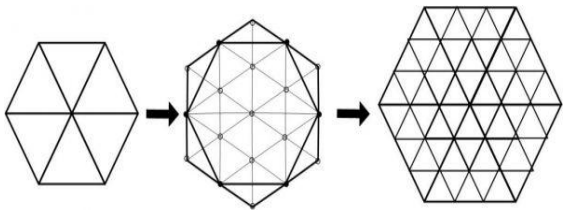

Figure 3: Clothing local mesh

The new high-quality clothing local mesh can be divided into: regular mesh, irregular mesh and semi-regular mesh. The regular grid is the simplest method but he most constrained method. On the other hand, an adaptive rule mesh is a collection of grids of different resolutions combined together. Due to the limitations of the topology, there will be cracks at the connections between different resolutions. This phenomenon is called T-connection. The grid shape is shown in Fig. 4. T-junctions can produce bad visual effects, affecting the results of realistic simulations. Adaptive irregular mesh is less constrained and can produce continuous mesh. The top-down approach is usually used to build irregular meshes, and the composite resolution hierarchy tree is pre-computed by merging into the finest mesh to the coarsest mesh. Before the pre-calculation of the hierarchical tree, considerable space is needed for storing the hierarchical tree.

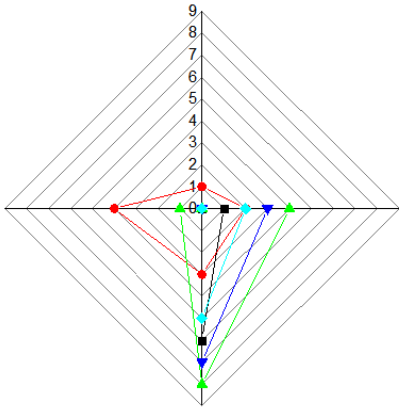

Figure 4: Clothing local T mesh structure of Self-adaptive processing

3.3 Tailoring analysis

Taking clothing designs as an example, in the three-dimensional clothing simulation design model, finding the sleeve and the cutting ring of the garment body is the key to automatic tailoring. Directly cutting the sleeves and clothing using a vertical plane passing through the underarm point produces a non-compliant cut loop. The specific cutting effect is shown in Fig. 5.

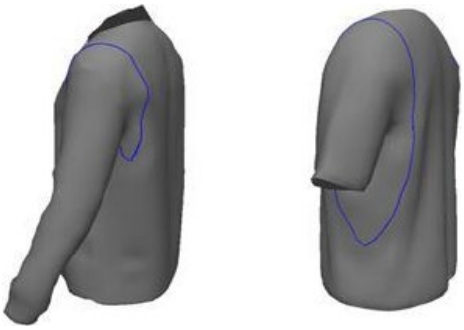

Figure 5: Inconformity requirements of the tailoring

The improved 3D human segmentation can be applied to many fields such as the generation of tight clothing, or also can be used to assess the degree of obesity in three-dimensional human body. In recent years, three-dimensional human body segmentation has been applied to approximate human body generation technology in research. Through the deformation of the human body simulation mechanism to get the shape of the target body, the desired tailoring effect has been achieved as shown in Fig. 6.

Figure 6: Ideal tailoring effect diagram

According to the three-dimensional long-sleeved shirt to cut three-dimensional human body, the three-dimensional human tailoring feature points are firstly determined. The three-dimensional human body needs to determine the cutting feature points that are different from the basic measurement feature points. The human body feature points correspond to the automatically cut three-dimensional clothing feature points. Different types of clothing need to generate different cutting feature points so as to form tailor path.

According to the three-dimensional long-sleeved shirt, there are five three-dimensional humans cutting feature points to be determined, namely, the neck point, the left subphrenic point, the right subphrenic point, and the bottom point. Through the five feature points, the three-dimensional body can be divided into head, left arm, right arm, left leg, right leg, and torso. The most easily found cut ring structures are the left lower point, the right lower point, and the bottom point. The determination of the lower left and lower right points is the same as that of the three-dimensional long-sleeved shirt in Fig. 5. First, a set of three-dimensional human cutting rings is obtained from the top-down horizontal section. In order to make a three-dimensional body part automatically match a three-dimensional virtual clothing piece, or to make a three-dimensional body piece automatically match with other three-dimensional body pieces, automatic three-dimensional body segmentation is required. The three-dimensional human cutting matching with the three-dimensional clothing pieces is similar to the three-dimensional clothing cutting method, and the feature points are obtained by cutting the ring structure, and the mesh is divided and grouped according to the feature points. The three-dimensional human cutting matching with other 3d human body blocks needs to determine the cutting path of the three-dimensional human body according to the position and number of the blocks, and then divides the groups and sorts them. In this section, firstly, the cutting of a three-dimensional human body according to a three-dimensional garment piece is introduced, including cutting a human body according to a

three-dimensional long-sleeved shirt and cutting the human body according to a trouser clip. It introduces the automatic segmentation of three-dimensional human bodies based on the number of three-dimensional human body segments to complete the construction of a new simulation model. A sample clothing designed based on three-dimensional image analysis garment simulation model is shown in Fig. 7.

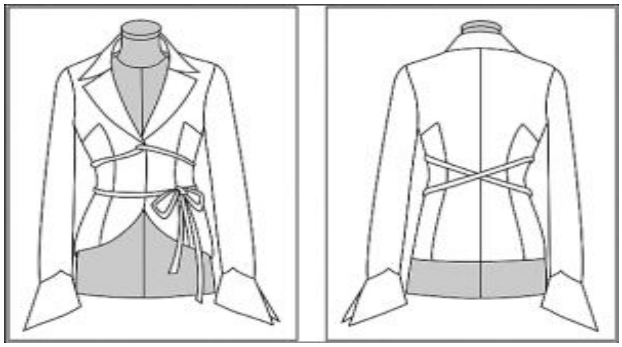

Figure 7: The sample garment is designed based on the three-dimensional image analysis clothing simulation model

4 Experimental results and analysis

To verify the practical value of new clothing simulation design model based on 3D image analysis technology, the following comparative experiments are designed, with two computers with 8G memory being used as experimental objects. One of them is equipped with a new clothing simulation design model as an experimental group, and the other is equipped with traditional clothing simulation design model as control group. The control variable method is used to record the data within a fixed period of time about the clear degree of fabric folds and the change in the shade of clothing color after the two sets of models.

4.1 Experimental parameter setting

In order to obtain stable data comparison results in the experiment, relevant parameters can be set according to Tab. 2 below.

Table 2: Experimental parameter setting table

Parameter name	Experience group	Control group
MSD/(%)	86.75	86.75
DCF/(%)	94.32	94.32
CBC/(%)	95.18	95.18
TID/(T)	4.65×1011	4.65×1011
MSI	0.83	0.83

In the above table, the MSD parameter represents the degree of model stability, the DCF parameter represents the ideal cloth crease clarity, the CBC parameter represents the ideal garment color shade, the TID parameter represents the total three-dimensional image data,

and the MSI parameter represents the model simulation index. In order to ensure the fairness of the experiment, the parameters of the experimental group and the control group are always the same.

4.2 Clarity comparison of cloth folds

On the premise of keeping other operating conditions unchanged, the change of wrinkling definition of the fabric under three working conditions of high frequency, intermedium frequency and low frequency was recorded with 10 minutes as the experiment time. Specific experimental values are shown in Tabs. 3-5.

Table 3: Cloth clearness comparison table (high frequency operation)

Experimental time/(min)	Degree of clarity of cloth fold in experimental group/(%)	Degree of clarity of cloth folds in the control group/(%)
0	53.28	17.85
1	56.77	18.43
2	61.09	19.61
3	64.35	21.32
4	70.21	22.47
5	70.21	24.68
6	70.21	28.53
7	70.21	32.76
8	77.46	37.29
9	82.58	40.72
10	89.54	45.60

Table 4: Cloth clearness comparison table (intermediate frequency operation)

Experimental time/(min)	Degree of clarity of cloth fold in experimental group/(%)	Degree of clarity of cloth folds in the control group/(%)
0	41.50	33.68
1	46.15	33.68
2	48.23	33.68
3	53.17	33.68
4	54.27	33.68
5	61.29	35.94
6	65.34	37.65
7	69.71	40.13
8	72.36	43.27
9	87.45	47.21
10	90.02	49.98

Table 5: Cloth clearness comparison table (Low frequency operation)

Experimental time/(min)	Degree of clarity of cloth fold in experimental group/(%)	Degree of clarity of cloth folds in the control group/(%)
0	73.08	44.28
1	80.55	41.06
2	83.12	38.97
3	85.70	37.91
4	87.33	35.24
5	90.85	34.37
6	93.29	34.12
7	95.64	32.57
8	95.64	31.95
9	95.64	30.83
10	95.64	30.01

Comparing Tabs. 3-5, it is seen that when the garment simulation design model maintains the high-frequency running state. With the increase of the running time, the clear degree of the cloth crease of the experimental group model shows increasing trend first, then stablizes, and then rises again. At 10 min, the clearness of the fabric crease reaches a maximum of 89.54%, which does not reach the expected value; the clarity degree of the fabric folds of the control group model shows a gradually increasing trend at 10 minutes, and the clarity of the fabric crease reaches a maximum of 45.60%, which is far lower than the experimental group. Compared with Tabs. 2 and 4, it can be presented that when the simulation design model of the garment is kept medium frequency state, as the running time increases, the degree of fabric wrinkle clarity of the experimental group is gradually rising. When the experiment time is 10 min, the clarity of the cloth folds reaches the maximum value of 90.02%, while the control group has not reached the expected value. The clear degree of cloth folds in the model presents a stable and then upwarding trend. When the experiment time is 10 min, the clarity of the cloth folds reaches the maximum value of 49.98%, far below the experimental group. Compared with Tabs. 2 and 5, it can be demonstrated that when the simulation design model maintains low frequency running state, the degree of fabric wrinkle clarity of the experimental group presents a rising and stable trend as the running time increases. When the experiment time reaches 7 min, the clarity of the cloth folds reaches the maximum value of 95.64%, which exceeds the expected value. The clear degree of cloth folds in the control group shows a gradual decreasing trend, and the clear degree of cloth fold to reaches a maximum of 44.28% at the beginning of the experiment, which is far lower than that of the experimental group.

4.3 Contrast of color and shade

On the premise of keeping the other operating conditions unchanged, using 10 min as the experimental time, the change of color brightness is recorded when the clothing simulation design models to maintain high frequency, medium frequency and low frequency operating state. The specific experimental conditions are shown in Figs. 8-10.

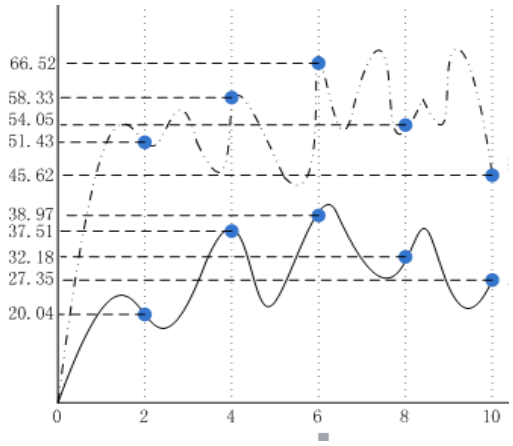

Figure 8: Color contrast diagram (high frequency operation)

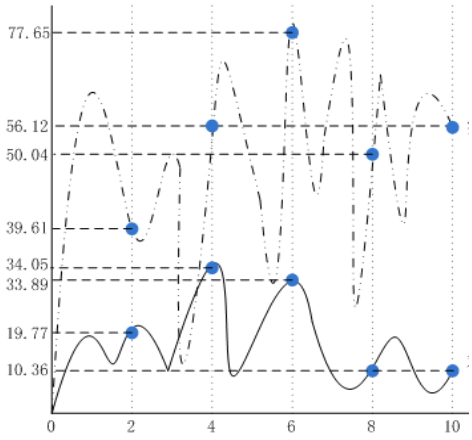

Figure 9: Color contrast diagram (intermediate frequency operation)

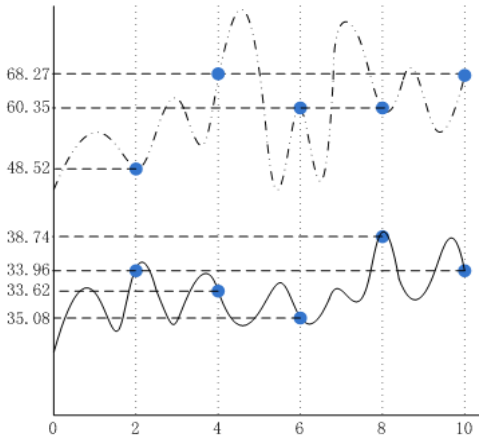

Figure 10: Color contrast diagram (low frequency operation)

As can be seen from the analysis in Fig. 8, with the increase of the running time, the color brightness of the experimental group increases first and then decreases with the increase of the running time. When the experiment time is 6 min, the color brightness reaches the maximum value of 66.52%, which does not exceed the target value. The color brightness of the control group also increased first and then decreased. When the experiment time is 8 min, the color brightness reaches 38.97%, much lower than that of the experimental group. The analysis of Fig. 9 shows that when the fashion simulation design model keeps the medium frequency running state, the color brightness increases first and then decreases as running time increases.

When the experiment time reaches 6 min, the maximum value of color brightness is 77.65%, which does not exceed the target value. When the experiment time is 4min, the color brightness reaches the maximum value of 34.05%, which is far lower than the experimental group. As shown in Fig. 10, when the model maintains low frequency running state, the color brightness of the model fluctuates by increasing and decreasing several times as the running time increases. When the experiment time reaches 4 minutes and 10min, the color brightness reaches the maximum value of 68.27%, which does not exceed the target value; The color brightness of the model decreases first, then increases and then decreases. When the experiment time is 8min, the color brightness reaches the maximum value of 38.74%, far below the test group.

5 Conclusion

Compared with the traditional model, the clothing simulation design model based on the 3D image analysis technology can fully improve the clarity of the cloth fold and the color brightness and so on. It saves the complicated and tedious calculation process in the construction of the model. Practicality, it saves a lot of time to select raw materials, and the images obtained from psimulation operation have higher authenticity. Generally speaking, this new model is of strong practical value.

Acknowledgement: Supported by the Science and Technology Public Welfare Project of Zhejiang Province.

Funding Statement: The authors received no specific funding for this study.

Conflicts of Interest: The authors declare that they have no conflicts of interest to report regarding the present study.

References

Bannas, P.; Li, Y.; Motosugi, U. (2017): Prior image constrained compressed sensing metal artifact reduction (PICCS-MAR): 2D and 3D image quality improvement with hip prostheses at CT colonography. *European Radiology*, vol. 26, no. 7, pp. 2039-2046.

Chen, G.; Ni, M.; Peng, H. (2017): Photoinitiation and inhibition under monochromatic green light for storage of colored 3d images in holographic polymer-dispersed liquid crystals. *ACS Applied Materials & Interfaces*, vol. 9, no. 2, pp. 1810-1819.

Deng, H.; Fitts, J. P.; Peters, C. A. (2017): Quantifying fracture geometry with X-ray tomography: technique of iterative local Thresholding (TILT) for 3D image segmentation. *Computational Geosciences*, vol. 20, no. 1, pp. 231-244.

Gaich, A.; Pötsch, M. (2017): 3D images for digital tunnel face documentation at TBM headings-Application at Koralmtunnel lot KAT2/3D ‐ Bilder zur digitalen Ortsbrustdokumentation bei TBM-Vortrieben-Anwendung beim Koralmtunnel Baulos KAT2. *Geomechanik Und Tunnelbau*, vol. 9, no. 3, pp. 210-221.

Goreczny, S.; Dryzek, P.; Moszura, T. (2017): 3D image fusion for live guidance of stent implantation in aortic coarctation-magnetic resonance imaging and computed tomography image overlay enhances interventional technique. *Postepy Kardiol Interwencyjnej*, vol. 13, no. 3, pp. 269-272.

Grosser, O. S.; Wybranski, C.; Kupitz, D. (2017): Improvement of image quality and dose management in CT fluoroscopy by iterative 3D image reconstruction. *European Radiology*, vol. 27, no. 9, pp. 3625-36288.

Hu, T. Z.; Hou, S. B. (2017): Optimization and Simulation of 3D digital image mosaic method for grotto architecture. *Computer Simulation*, vol. 34, no. 12, pp. 250-253.

Journal of Internet Technology, vol. 19, no. 3, pp. 959-967.

Karlsson, L.; Thunberg, P.; With, A. (2017): 3D image-based adapted high-dose-rate brachytherapy in cervical cancer with and without interstitial needles: measurement of applicator shift between imaging and dose delivery. *Journal of Contemporary Brachytherapy*, vol. 9, no. 1, pp. 52-58.

Keall, P. J.; Ng, J. A.; Juneja, P. (2017): Real-time 3D image guidance using a standard linac: measured motion, accuracy, and precision of the first prospective clinical trial of kilovoltage intrafraction monitoring-guided gating for prostate cancer radiation therapy. *International Journal of Radiation Oncology Biology Physics*, vol. 94, no. 5, pp. 1015-1021.

Kim, Y.; Modrick, J. M.; Pennington, E. C. (2017): Commissioning of a 3D image-based treatment planning system for high-dose-rate brachytherapy of cervical cancer. *Journal of Applied Clinical Medical Physics*, vol. 17, no. 2, pp. 405-426.

Lie, D.; Trivedi, A. R.; Mukhopadhyay, S. (2017): Impact of heterogeneous technology integration on the power, performance, and quality of a 3D image sensor. *IEEE Transactions on Multi-Scale Computing Systems*, vol. 2, no. 1, pp. 61-67.

Majchrowicz, M.; Kapusta, P.; Jackowskastrumiłło, L. (2017): Optimization of distributed Multi-Node, Multi-Gpu, heterogeneous system for 3D image reconstruction in electrical capacitance tomography. *Image Processing & Communications*, vol. 21, no. 3, pp. 81-90.

Matsubara, M.; Hashimoto, T. (2017): The fundamental research on the improvement of measurement range in 3D image measurement of human leg using mirrors. *IEEJ Transactions on Electronics Information & Systems*, vol. 137, no. 3, pp. 459-466.

Nitzken, M.; Beache, G. M.; Ismail, M. (2017): Improving full-cardiac cycle strain estimation from tagged CMR by accurate modeling of 3D image appearance characteristics. *Egyptian Journal of Radiology & Nuclear Medicine*, vol. 47, no. 1, pp.

83-94.

Ribeiro, I.; Janssen, H.; De, B. (2017): Long term experience with 3D image guided brachytherapy and clinical outcome in cervical cancer patients. *Radiotherapy & Oncology Journal of the European Society for Therapeutic Radiology & Oncology*, vol. 120, no. 3, pp. 447-454.

Schwerter, M.; Lietzmann, F.; Schad, L. R. (2017): A novel approach for a 2D/3D image registration routine for medical tool navigation in minimally invasive vascular interventions. *Zeitschrift Fur Medizinische Physik*, vol. 26, no. 3, pp. 259-269.

Sun, Y.; Li, Q. M.; Lowe, T. (2017): Investigation of strain-rate effects on the compressive behavior of closed-cell aluminum foam by 3D image-based modelling. *Materials & Design*, vol. 89, no. 11, pp. 215-224.

Wang, Q.; Wei, M.; Chen, X. (2017): Joint encryption and compression of 3D images based on tensor compressive sensing with non-autonomous 3D chaotic system. *Multimedia Tools & Applications*, vol. 77, no. 10, pp. 1-20.

Wei, F.; Wen, X. Z.; Xu, J.; Zhu, J. Z. (2018): MeteCloud: meteorological cloud computing platform for mobile weather forecasts based on energy-aware scheduling.

Wei, F.; Wen, X. Z.; Xu, J.; Zhu, J. Z. (2019): CSDA: a novel cluster-based secure data aggregation scheme for WSNs. *Cluster Computing*, vol. 3, no. 22, pp. 5233-5244.

Yong, J. J.; Kim, H. G.; Yong, M. R. (2017): Critical binocular asymmetry measure for the perceptual quality assessment of synthesized stereo 3D images in view synthesis. *IEEE Transactions on Circuits & Systems for Video Technology*, vol. 26, no. 7, pp. 1201-1214.